Chandra Observations of Cygnus A: Magnetic Field Strengths in the Hot Spots of a Radio Galaxy

A. S. Wilson[1], A. J. Young

Astronomy Department, University of Maryland, College Park, MD 20742;

wilson@astro.umd.edu, ayoung@astro.umd.edu

and

P. L. Shopbell

Department of Astronomy, Mail Code 105-24, California Institute of Technology, Pasadena, CA 91125; pls@astro.caltech.edu

Received July 28, 2000; accepted September 18, 2000

To be published in the Astrophysical Journal (Letters)

---

[1] Adjunct Astronomer, Space Telescope Science Institute, 3700 San Martin Drive, Baltimore, MD 21218; awilson@stsci.edu

ABSTRACT

We report X-ray observations of the powerful radio galaxy Cygnus A with the Chandra X-ray Observatory. This letter focuses on the radio hot spots, all four of which are detected in X-rays with a very similar morphology to their radio structure. X-ray spectra have been obtained for the two brighter hot spots (A and D). Both are well described by a power law with photon index $\Gamma = 1.8 \pm 0.2$ absorbed by the Galactic column in the direction of Cygnus A. Thermal X-ray models require too high gas densities and may be ruled out. The images and spectra strongly support synchrotron self-Compton models of the X-ray emission, as proposed by Harris, Carilli & Perley on the basis of ROSAT imaging observations. Such models indicate that the magnetic field in each of the brighter hot spots is 1.5×10^{-4} gauss, with an uncertainty of a few tens of percent. This value is close to the equipartition field strengths assuming no protons are present. The possibility that the X-rays are synchrotron radiation is briefly discussed, but not favored. We speculate that production of the $\gamma \sim 10^7$ electrons necessary for X-ray synchrotron radiation from hot spots is inhibited when the external gas density is high, as is the case when the radio galaxy is within a cooling flow.

Subject headings: galaxies: active – galaxies: individual (Cygnus A) – galaxies: jets – galaxies: nuclei – magnetic fields – X-rays: galaxies

1. INTRODUCTION

The spectral emissivity of optically thin synchrotron radiation is proportional to $\mathrm{n_{e0}B^{(p+1)/2}}$, where $\mathrm{n_{e0}}$ is the constant in the relativistic electron number density spectrum ($\mathrm{n_e}(\gamma)d\gamma = \mathrm{n_{e0}}\gamma^{-\mathrm{p}}\mathrm{d}\gamma$, $\gamma = \mathrm{E/m_ec^2}$) and B is the magnetic field strength. Observations of synchrotron sources allow this product to be determined, but not n_{e0} and B separately. It is common practice to quote the equipartition magnetic field, B_{eq}, the field for which the energies in relativistic particles and magnetic field are equal; this field is close to that at which the total energy in relativistic particles plus magnetic field is a minimum. This inability to obtain a direct measurement of the magnetic field strength has seriously hampered progress in understanding cosmic synchrotron sources.

The relativistic electrons will inevitably scatter any photons in the source through the inverse Compton process. The emissivity of inverse Compton radiation depends on the electron energy spectrum and the radiation spectrum, the latter being an observable quantity for an isotropic source. Detection of inverse Compton radiation thus permits n_{e0} to be measured and hence B from the synchrotron spectrum. If the photons being scattered are the synchrotron radiation itself, the resulting emission is called synchrotron self-Compton (SSC) radiation.

For a typical extended non-thermal radio source, much of the inverse Compton emission is expected to be radiated at X-ray energies. Unfortunately, the existence of other mechanisms that generate X-rays - thermal and synchrotron emissions - and the poor spatial and spectral resolutions of previous X-ray observatories has precluded the use of this method to measure magnetic field strengths in either supernova remnants or extragalactic radio sources.

In this paper, we present the first results of a study of the nearby ($z = 0.0562$), powerful radio galaxy Cygnus A with the Chandra X-ray Observatory. We focus on the X-ray emission of the radio hotspots. Previously, Harris, Carilli & Perley (1994, hereafter HCP) detected soft X-ray emission from the dominant western and eastern hot spots (termed A and D by Hargrave & Ryle 1974) with the High Resolution Imager of the ROSAT Observatory. They compared the measured X-ray fluxes with predictions of SSC models and argued that the magnetic fields in the hot spots are quite close to the equipartition values, calculated assuming no contribution from relativistic protons. The angular resolution of the ROSAT HRI was $\simeq 5''$, so the point spread function included both weaker radio structures (such as the fainter hot spots B and E - cf. Perley, Dreher & Cowan 1984) and thermal emission from the cluster gas. More significantly, the detector had almost no spectral resolution so HCP were unable to measure the X-ray spectra of the hot spots. The Chandra observations overcome these limitations. The sub arc second angular resolution and high sensitivity of Chandra have allowed detection and spatial resolution of X-ray emission from all four hot spots. We also report the X-ray spectra of the two brightest hot spots (A and D), finding excellent agreement with the predictions of the SSC model. This agreement strongly favors the SSC model, but does not rule out a contribution from X-ray synchrotron emission, as we briefly discuss. We use $H_0 = 50$ km s^{-1} Mpc^{-1} and $q_0 = 0$ throughout. Other aspects of the Chandra results on Cygnus A will be discussed elsewhere.

2. OBSERVATIONS AND REDUCTION

Cygnus A was observed by the Chandra X-ray Observatory on May 21 2000 (sequence number 700032, obsid 360) using the Advanced CCD Imaging Spectrometer (ACIS) spectroscopic array. The nucleus was centered $20''$ in the –Y direction from the location of best focus on chip S3. All of the regions of radio emission from Cyg A were imaged on S3. The total good time interval was 34.7 ksecs taken with the default frame time of 3.2 secs. The data extraction and analysis have been performed using version 1.1.3 of the CIAO software and version 11.0 of XSPEC. A new level 2 events file, with the correct gain map (acisD2000-01-29gainN0001.fits), was made from the events file supplied by the Chandra Science Center. The data were inspected for bad aspect and high background times, but none were found. The response matrix file and ancillary response file were initially obtained from calibration data obtained with the chip at -110C. The spectra were recalculated with calibration data for a temperature of -120C (the temperature during the observations) when these became available, but were insignificantly different from those obtained with the -110C calibration. The counts used to obtain the spectra of hot spots A and D were taken from circular regions of radii $2''.3$ and $2''.2$, respectively, with background taken from annular regions of width $\simeq 2''$ concentric with the source region.

3. RESULTS

3.1. Morphology

Fig. 1 is a grey scale plot of the X-ray emission from the region of the radio source. The Chandra astrometry shows that the nuclear X-ray source agrees with the nuclear radio source to within $1''.4$. When the X-ray and radio nuclei are aligned, the compact X-ray sources at the SE and NW edges of Fig. 1 coincide with the corresponding radio hot spots to within $0''.5$. Fig 2 shows X-ray contours on a grey scale of a 6 cm image with resolution $0''.35$ (Perley, Dreher & Cowan 1984; Carilli & Barthel 1996) in the vicinities of the western (A and B) and eastern (D and E) hot spots.

As may be seen in Fig. 2, the extents and morphologies of the X-ray and radio hot spots are very similar, with the directions of elongation agreeing to within a few degrees. Despite the somewhat lower resolution of the X-ray image, it is clear that the X-ray emission comes from essentially the same region as the radio emission in each hot spot.

3.2. Spectra

Hot spots B and E are too weak to obtain reliable X-ray spectra, so we focus on A and D. The results of modelling each spectrum with an absorbed power law are shown in Table 1. In both cases, the absorbing column is $\mathrm{N_H} = 3.3 \times 10^{21}$ cm^{-2}, in excellent agreement with the Galactic column (3.3×10^{21} cm^{-2}, HCP) in the direction of Cygnus A. The photon indices are similar at $\Gamma = 1.8 \pm 0.2$. Alternatively, the spectra may be well described by a Raymond-Smith thermal plasma model with temperatures 4.9 keV (A) and 6.0 keV (D).

3.3. X-ray Emission Mechanism

A thermal model requires a density of 0.5 cm^{-3} in each hot spot. This value is 10^3 times larger than the upper limit to the internal density in the hot spots from the absence of Faraday depolarization (Dreher, Carilli & Perley 1987). It is also hard to understand how such a high density could be produced in the hot spots given that the density of the intracluster medium near them is only $\simeq 0.01$ cm^{-3} (HCP; Reynolds & Fabian 1996). We conclude that a thermal model for the X-ray emission of the hot spots is untenable.

In view of the success of a SSC model in reproducing the intensity of the soft X-ray emission (HCP), it is natural to check whether the model can also reproduce the X-ray spectra. From the radio spectra of the hot spots (Carilli et al. 1991), we first calculated the internal radiant energy density in the hot spots, modelled as uniformly emitting spheres, from $\epsilon_\mathrm{R} = 3\mathrm{L_R R}/4\mathrm{cV}$, where $\mathrm{L_R}$ is the total radio luminosity, R and V are the radius and volume of the hot spot, and c is the speed of light. The results are $\epsilon_\mathrm{R} \simeq 3 \times 10^{-11}$ erg cm^{-3} for each hot spot. These values are $\simeq 100$ times larger than the energy density of the microwave background ($\epsilon_\mathrm{M} \simeq 4 \times 10^{-13}$ erg cm^{-3}), showing that an SSC model is indeed appropriate. The radiant energy densities in the hot spots are, however, $\simeq 100$ times smaller than that in the magnetic field ($\epsilon_{\rm B} \simeq 3 \times 10^{-9}$ erg cm^{-3}) assuming equipartition and no relativistic protons. Thus the rate of energy loss by the electrons to synchrotron radiation will be $\simeq$ 100 times larger than to SSC radiation.

To calculate the SSC spectra, we have used the code of Band & Grindlay (1985, 1986) which assumes spherical geometry. Following Carilli et al. (1991), the radio spectrum of each hot spot was modelled as a broken power law with spectral index $\alpha = 0.55$ (hot spot A, S $\propto \nu^{-\alpha}$) and 0.50 (hot spot D) below the break frequency and 1.05 (A) and 1.0 (D) above it. Such a change in slope of 0.5 is expected in models of continuous injection of electrons accompanied by synchrotron losses (Kardashev 1962). The emitting region was taken to be a uniform sphere in each case.

The results of the modelling are given in Table 2 and compared with the Chandra spectra in Figs 3a and b. As may be seen, the predicted SSC radiation is in excellent agreement with the Chandra-observed spectrum for a magnetic field of 1.5 $\times$ 10^{-4} gauss in each hot spot, in good agreement with the results of HCP based on the X-ray intensity. This value may be compared with the equipartition values of 2.8 $\times$ 10^{-4} gauss (hot spot A) and 2.5 $\times$ 10^{-4} gauss (D), calculated assuming no relativistic protons, the broken power-law spectra of Carilli et al. (1991), low frequency cut-offs at 10 MHz and high frequency cut-offs at 400 GHz. The calculated field is insensitive to the precise cut-off frequencies. The SSC model predicts spectral steepening towards higher energies within the Chandra band. We have searched for this effect, finding a hint of a larger value of Γ in the 2.5 - 6 keV band than in the 0.7 - 2.5 keV band for hot spot D. However, this difference in photon indices is not significant.

Uncertainty in the magnetic field obtained with the SSC model results from a number of factors, including a) the idealisation of the hot spots as uniform spheres of known radii, b) the errors in the Chandra-measured spectra, and c) modelling the radio spectrum of each hot spot as a broken power law, with sharp changes in the slopes of both the electron energy and the synchrotron radiation spectra at the break energy and frequency. Comparison of the formulae for synchrotron and inverse Compton radiation indicates that changing the volume by a factor of 2 changes B by $\sim$ 30%. The normalisation of the Chandra spectra are uncertain by $\simeq$ 17 - 28% (Table 1). An error of 25% in SSC flux changes B by $\simeq$ 15%. Lastly, the idealised treatment of the electron energy and synchrotron spectra around the break is estimated to contribute $\lesssim$ 10% uncertainty. The precise locations and shapes of the high energy cut-offs have little effect on the SSC spectra in the Chandra band. We conclude that the error in the magnetic fields derived from the SSC model amounts to a few tens of percent.

4. CONCLUDING REMARKS

The X-ray spectra of the two brightest radio hot spots (A and D) of Cygnus A are in excellent agreement with an SSC model in which the magnetic field is 1.5×10^{-4} gauss. This value is close to the equipartition fields of 2.8×10^{-4} and 2.5×10^{-4} gauss for hot spots A and D respectively, calculated assuming no relativistic protons are present (i.e. the ratio of the energy density in relativistic protons to that in electrons, K = 0). The most straightforward interpretation is that the relativistic gas is an electron-positron plasma and is close to equipartition with the magnetic field. If, on the other hand, there is significant energy in relativistic protons (e.g. K $\sim$ 100, a value appropriate to the relativistic protons and electrons observed at the top of the Earth's atmosphere) and the X-rays are still SSC radiation, the energy density in relativistic protons must exceed that in the magnetic field. It is notable that the magnetic field cannot be less than 1.5×10^{-4} gauss since the SSC radiation would then exceed the observed X-radiation.

The alternative is that $B > 1.5 \times 10^{-4}$ gauss in which case the predicted SSC emission would be too weak to account for the observed X-ray emission. The X-rays would then have to be synchrotron radiation, as we have recently argued for the jet and hot spot of Pictor A (Wilson, Young & Shopbell 2001). Synchrotron X-ray emitting electrons in hundreds of microgauss strength magnetic fields have synchrotron half lives of order years. They must thus be continuously accelerated within the hot spots. Here, again, there are two options - direct electron acceleration to $\gamma \simeq 10^7$ - 10^8 or a "proton-induced cascade". In the latter process (e.g. Mannheim, Krülls & Biermann 1991; Biermann 1996), ultrahigh energy protons ($\gamma_{\rm p} \sim 10^{11}$), perhaps shock accelerated, interact with photons to initiate a cascade, which eventually yields relativistic electron-positron pairs. The peak of the radiation from this process is at $\sim$ MeV energies, and the spectral index predicted in the Chandra band is $\alpha \simeq 0.7$ (Mannheim, Krülls & Biermann 1991), in agreement with the spectral index observed. Observations at higher energies than the Chandra band, where the proton-induced cascade predicts a harder spectrum than the SSC model, are needed to distinguish the two processes.

X-ray emission has now been detected from a number of hot spots in radio galaxies. For three galaxies - 3C 123 (Hardcastle 2000), 3C 295 (Harris et al. 2000) and Cygnus A (present paper), the X-ray emission is well explained by SSC emission from the radio synchrotron-emitting electrons with a magnetic field close to equipartition for $K = 0$. In three other galaxies - Pictor A (Wilson, Young & Shopbell 2001), 3C 120 (Harris et al. 1999) and 3C 390.3 (Harris, Leighly & Leahy 1998) - the X-ray emission is orders of magnitude too strong to be SSC emission with an equipartition magnetic field. Further, the X-ray spectrum of Pictor A predicted by the SSC model disagrees with that observed. In these cases, the X-rays are probably synchrotron radiation from $\gamma \sim 10^7$ electrons. It is notable that 3C 295 and Cygnus A are in clusters with prominent cooling flows, while 3C 123 is in a cluster with strong, extended X-ray emission and thus may be within a cooling flow. In contrast, Pictor A, 3C 120 and 3C 390.3 are not in cooling flows. It is tempting to speculate that the presence of high density surrounding gas may inhibit production of X-ray synchrotron emitting electrons in hot spots. Several processes may be relevant to this effect, e.g. hot spots propagating into the dense gas of a cooling flow should have lower outward velocities, and there may be more entrainment of thermal gas into the jet and hot spot. Such effects may reduce the efficiency with which $\gamma \sim 10^7$ electrons are accelerated. Future Chandra X-ray observations of additional radio galaxies should shed light on this issue.

We are grateful to Rick Perley for providing the VLA 6 cm map of Cygnus A in numerical form. We also wish to thank the staff of the Chandra Science Center, especially Dan Harris and Shanil Virani, for their help.

REFERENCES

Band, D. L. & Grindlay, J. E. 1985, ApJ, 298, 128

Band, D. L. & Grindlay, J. E. 1986, ApJ, 308, 576

Biermann, P. L. 1996, in “Cygnus A - Study of a Radio Galaxy”, Eds. C. L. Carilli & D. E. Harris, p 139 (Cambridge University Press)

Carilli, C. L., Perley, R. A., Dreher, J. W. & Leahy, J. P. 1991, ApJ, 383, 554

Carilli, C. L. & Barthel, P. D. 1996, A&A Review, 7, 1

Dreher, J. W., Carilli, C. L. & Perley, R. A. 1987, ApJ, 316, 611

Hardcastle, M. 2000, talk given at meeting “Particles and Fields in Radio Galaxies”, Oxford, U. K. Aug. 3 - 5.

Hargrave, P. J. & Ryle, M. 1974, MNRAS, 166, 305

Harris, D. E., Carilli, C. L. & Perley, R. A. 1994, Nature, 367, 713 (HCP)

Harris, D. E., Leighly, K. M. & Leahy, J. P. 1998, ApJ, 499, L149

Harris, D. E., Hjorth, J., Sadun, A. C., Silverman, J. D. & Vestergaard, M. 1999, ApJ, 518, 213

Harris, D. E. et al. 2000, ApJ, 530, L81

Kardashev, N. S. 1962, Sov. Astr. (AJ), 6, 317

Mannheim, K., Krülls, W. M. & Biermann, P. L. 1991, A&A, 251, 723

Meisenheimer, K., Yates, M. G. & Röser, H.-J. 1997, A&A, 325, 57

Perley, R. A., Dreher, J. W. & Cowan, J. J. 1984, ApJ, 285, L35

Reynolds, C. S. & Fabian, A. C. 1996, MNRAS, 278, 479

Wilson, A. S., Young, A. J. & Shopbell, P. L. 2001, ApJ, 546 (in press for Jan 10 2001 issue)

This manuscript was prepared with the AAS LaTeX macros v5.0.

Table 1. Spectral fits to the X-ray emission of the hot spots[a]

Hot spot	N_H[b]	Γ	Normalization[c]	χ^2 / d.o.f.
A	$3.26^{+0.74}_{-0.61}$	$1.84^{+0.22}_{-0.19}$	$\left(2.93^{+0.81}_{-0.63}\right) \times 10^{-5}$	27 / 27
D	$3.30^{+0.63}_{-0.26}$	$1.75^{+0.19}_{-0.17}$	$\left(4.40^{+0.97}_{-0.77}\right) \times 10^{-5}$	31 / 39

[a] Errors are 90% confidence for single parameter of interest.

[b] 10^{21} atom cm^{-2}.

[c] Photons keV^{-1} cm^{-2} s^{-1} at 1 keV.

Table 2. Parameters of synchrotron self-Compton models

Hot spot	B (Gauss)	n_{e0} (cm^{-3})	α	γ_{break}	γ_{max}	Radius (kpc)
A	1.5×10^{-4}	1.9×10^{-3}	0.55	3.5×10^{3}	5.0×10^{4}	2.0
D	1.5×10^{-4}	5.5×10^{-4}	0.50	5.5×10^{3}	5.0×10^{4}	2.2

Fig. 1.— A grey scale representation of the Chandra X-ray image of Cygnus A. The shading is proportional to the square root of the intensity. Coordinates are for epoch J2000.0 both here and in Fig. 2.

Fig. 2.— (a) X-ray emission (contours) superposed on a 6 cm VLA radio map (grey scale) of the region of the western hot spots (A, the brighter, and B, $\simeq 6''$ SE of A). Contours are plotted at 2, 4, 8, 12, 16, 24 and 32 counts per pixel ($0\farcs5 \times 0\farcs5$). The grey scale is proportional to the square root of the radio brightness. (b) As Fig. 2a, but for the eastern hot spots (D, the brighter, and E, $\simeq 4''$W of D). Contours are plotted at 2, 4, 8, 12, 16, 24, 32, 40, 48 and 56 counts per pixel.

Fig. 3.— (a) Spectrum of hot spot A. The points show the radio fluxes and the line through them the model of the synchrotron radiation. The "bow tie" is the Chandra measured boundary of the X-ray spectrum (these error lines are 90% confidence after freezing N_H at its best fit value, which coincides with the Galactic column). The solid line is the predicted SSC spectrum for $\gamma_{min} = 1$ and the dashed line for $\gamma_{min} = 100$. (b) As Fig. 3a, but for hot spot D. The near infrared and optical upper limits are from Meisenheimer, Yates & Röser (1997), including their allowance for obscuration.

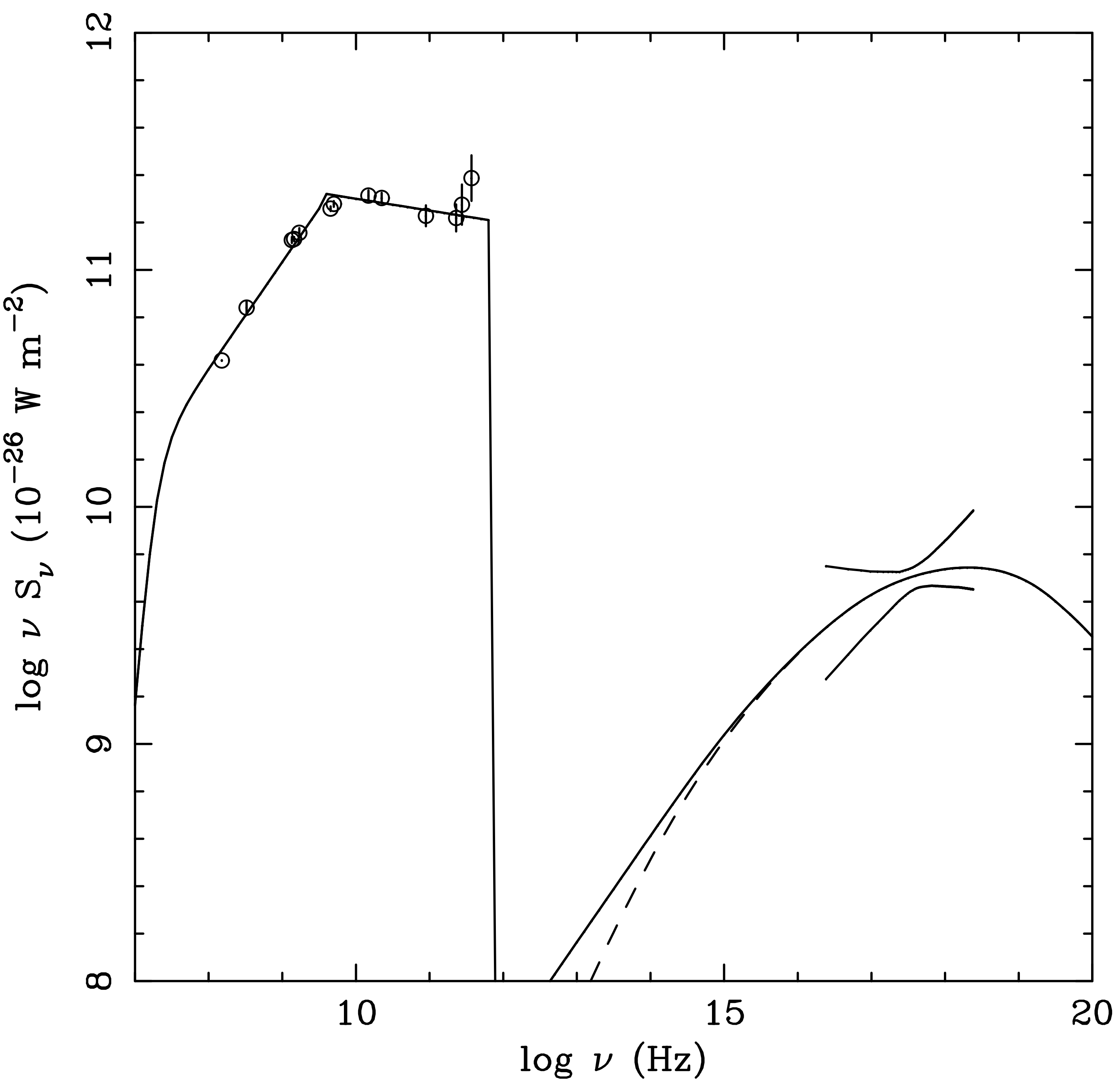
12
11
10
9
8
log ν S_ν (10^{-26} W m^{-2})
10
15
20
log ν (Hz)

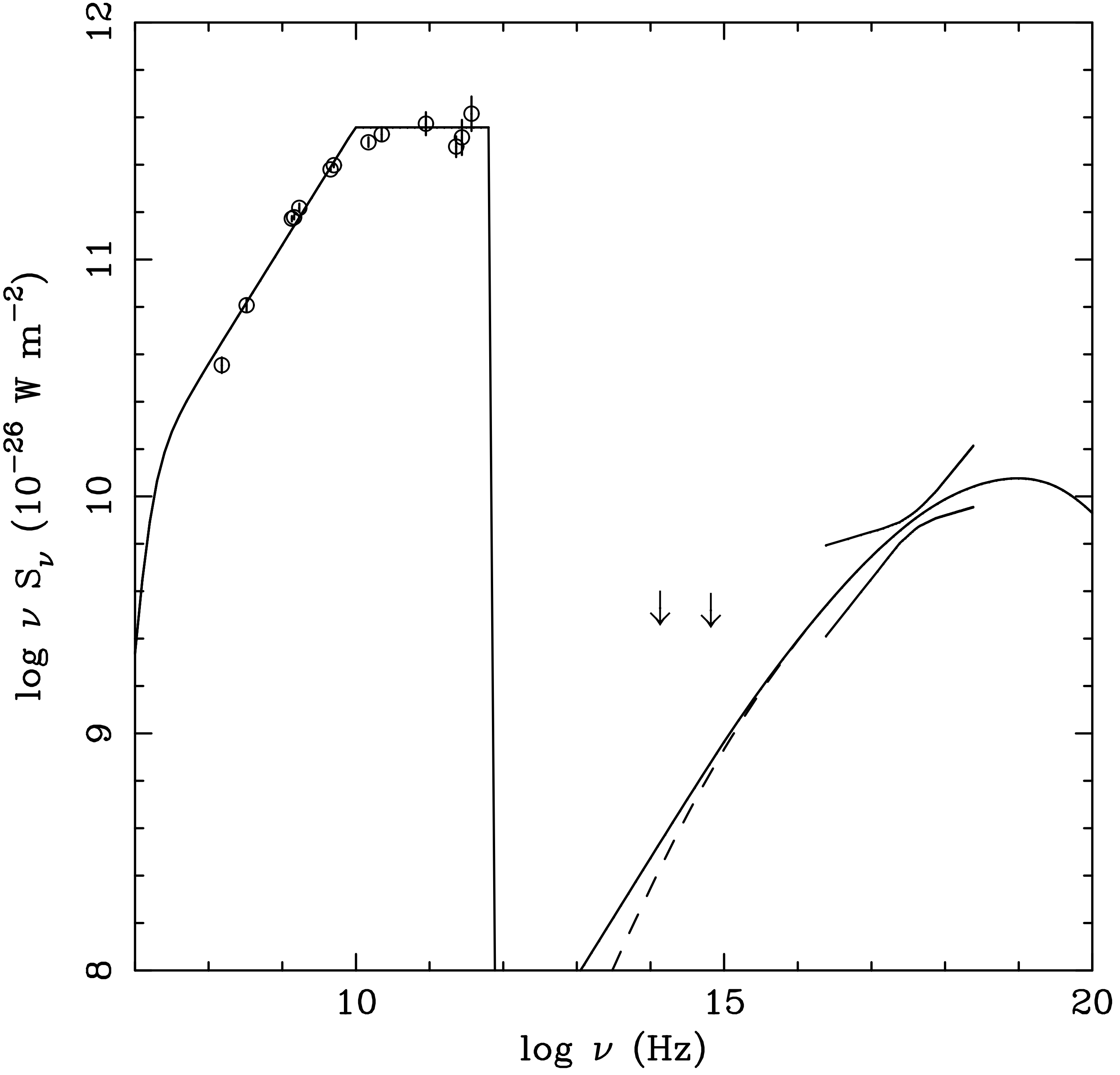
12
11
10
9
8
10
15
20
log ν (Hz)
log ν S_ν (10^-26 W m^-2)